Society of Medical Education & Research

2021, Volume 1, Page No: 189-205
ISSN: 3108-4834

Archive of International Journal of Cancer and Allied Science

Upregulation of PHOX1 Driven by Hypomethylation Accelerates Gastric Cancer Progression through NGFR Transactivation

Ahmed Youssef El Sayed[1]*, Mona Ibrahim Hassan[1]

[1]Department of Clinical Oncology, Faculty of Medicine, Cairo University, Cairo, Egypt.

***E-mail** ✉ ahmed.elsayed.onco@gmail.com

Abstract

Gastric cancer (GC) continues to rank among the primary causes of cancer-associated deaths worldwide, with few effective treatments available and incompletely elucidated molecular pathways. By conducting comprehensive analyses of TCGA and GEO databases, along with validation in clinical samples, we detected recurrent elevated expression of the transcription factor PHOX1 in GC specimens. This upregulation was strongly linked to higher T/M stages and unfavorable patient outcomes. We established that hypomethylation of the PHOX1 promoter, especially at the CpG site cg04123776, is responsible for its overexpression in GC. In vitro experiments showed that PHOX1 overexpression promoted GC cell growth, migration, and invasiveness, whereas PHOX1 silencing suppressed these oncogenic properties. Furthermore, orthotopic xenograft studies verified its role in facilitating liver metastasis from GC cells. At the molecular level, RNA sequencing, ChIP assays, and luciferase reporter experiments revealed that PHOX1 directly enhances transcription of the Nerve Growth Factor Receptor (NGFR). Rescue studies using NGFR-targeted siRNA and an ERK1/2 inhibitor confirmed that PHOX1 exerts its oncogenic effects through NGFR and the downstream ERK1/2 pathway. Overall, this work identifies PHOX1 as an oncogene responsive to methylation changes in GC, driving tumor advancement via NGFR transactivation. The PHOX1-NGFR-ERK1/2 pathway could represent a potential target for treating metastatic GC.

Keywords: PHOX1, Hypomethylation, Gastric cancer, NGFR

Introduction

Gastric cancer (GC) ranks as one of the most common and deadly cancers globally, marked by scarce treatment choices and poor survival rates [1]. Data from the Global Cancer Observatory indicate more than 1 million new diagnoses and around 700,000 fatalities each year [2]. Although improvements have occurred in detection and therapy, the 5-year survival for advanced GC is still low, as metastasis drives nearly 90% of deaths from the disease [3, 4]. These challenges highlight the critical demand for new insights into the molecular factors promoting GC advancement and spread.

The paired-related homeobox 1 (PHOX1), alternatively termed PRRX1, functions as a vital controller of embryonic growth and cellular differentiation [5, 6]. It has lately been recognized as a tumor modulator that varies by context. Growing data suggest PHOX1 affects cancer development via processes like epithelial-mesenchymal transition [7], preservation of cancer stem cell properties [8], and control of blood vessel formation [9]. Its effects differ by cancer type: PHOX1 promotes metastasis in osteosarcoma through TGF-β and Wnt/β-catenin activation [10] and supports glioma stem cells by transactivating DRD2 [11], but suppresses tumors in clear cell renal carcinoma by blocking vascular mimicry [12]. In GC, several reports have associated PHOX1 elevation with later stages and worse prognosis [13–15], yet its exact control mechanisms and targets are not well

Access this article online https://smerpub.com/

Received: 11 September 2021; **Accepted:** 07 December 2021

Copyright CC BY-NC-SA 4.0

How to cite this article: El Sayed AY, Hassan MI. Upregulation of PHOX1 Driven by Hypomethylation Accelerates Gastric Cancer Progression through NGFR Transactivation. Arch Int J Cancer Allied Sci. 2021;1:189-205. https://doi.org/10.51847/GBrHKFolZA

defined, especially regarding epigenetic influences and GC-unique pathways.

Epigenetic changes are central to cancer initiation and progression [16]. DNA methylation, in particular, regulates gene activity by modifying chromatin structure, DNA stability, and protein-DNA binding without altering the sequence [17, 18]. Promoter CpG island hypermethylation often silences tumor suppressors, while hypomethylation can activate oncogenes [17]. Due to its reversibility, DNA methylation is an attractive cancer therapy target, with much effort focused on demethylating silenced suppressors [18]. Despite PHOX1's oncogenic roles in various cancers, its epigenetic control in tumors is underexplored. It remains unknown if promoter methylation governs PHOX1 levels and how this relates to prognosis, meriting deeper study. In this study, we show that PHOX1 undergoes epigenetic activation in GC via promoter hypomethylation at cg04123776, with higher expression tied to advanced T/M stages and reduced survival. Functionally, PHOX1 fuels GC cell growth, invasion, and metastasis by directly upregulating NGFR transcription, which activates the ERK1/2 oncogenic cascade. These data position PHOX1 as a methylation-regulated oncogene in GC and highlight the PHOX1-NGFR-ERK1/2 pathway as a candidate for targeted therapy. Our results offer key knowledge for biomarker development and tailored treatments in GC.

Results and Discussion

PHOX1 is upregulated in GC and correlated with poor patient survival

To pinpoint genes linked to GC advancement, we carried out differential expression analysis on four separate datasets (GSE54129, GSE79973, GSE118916, and GSE19826) with the limma R package. Using strict thresholds (|log2FC| > 2, adjusted p-value < 0.05), we found nine genes consistently altered (TFF2, VSIG1, SOSTDC1, GKN2, GKN1, PHOX1, PGC, ATP4B, FUT9) in all datasets **(Figures 1a)**. LASSO regression combined with univariate Cox regression then singled out PHOX1 as the top prognostic indicator for GC progression **(Figures 1b–1d)**.

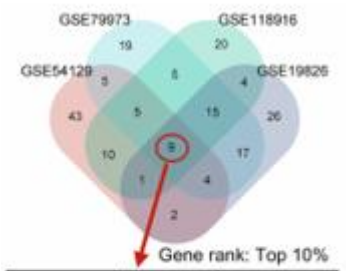

TFF2	GKN2	PGC
VSIG1	GKN1	ATP4B
PHOX1	FUT9	SOSTDC1

a)

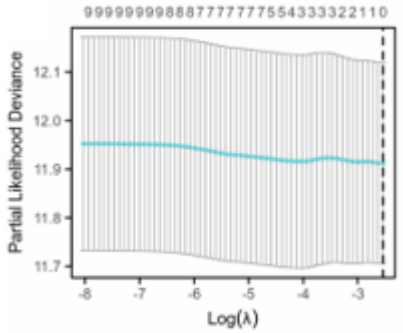

b)

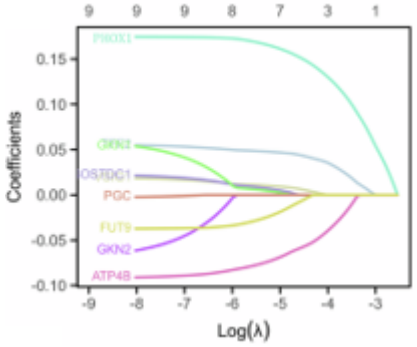

c)

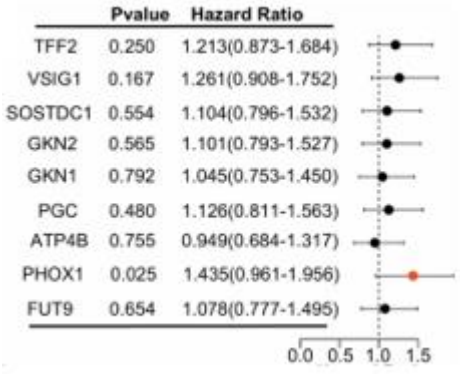

d)

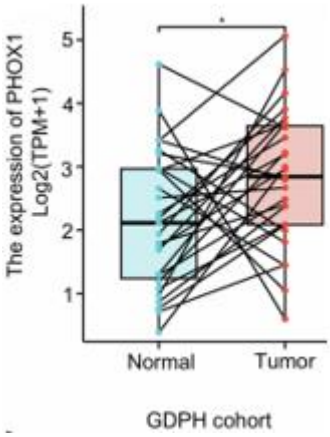
The expression of PHOX1
Log2(TPM+1)
Normal
Tumor
GDPH cohort

e)

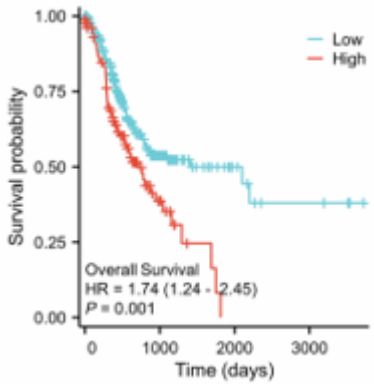
Survival probability
Low
High
Overall Survival
HR = 1.74 (1.24 - 2.45)
P = 0.001
Time (days)

f)

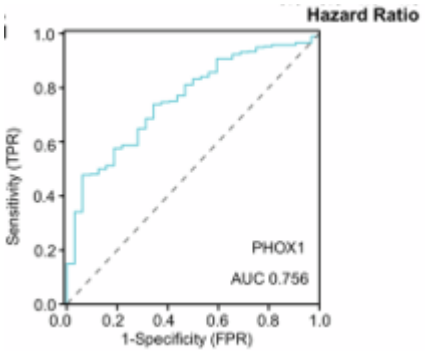
Hazard Ratio
Sensitivity (TPR)
1-Specificity (FPR)
PHOX1
AUC 0.756

g)

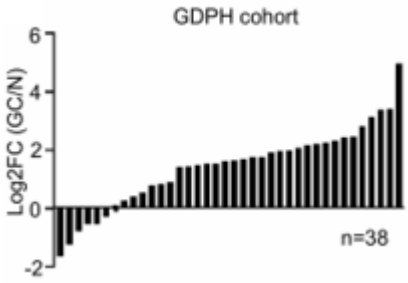
GDPH cohort
Log2FC (GC/N)
n=38

h)

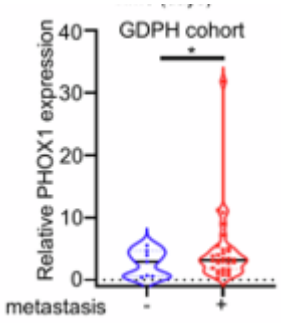
GDPH cohort
Relative PHOX1 expression
metastasis

i)

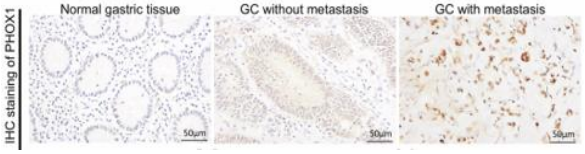
IHC staining of PHOX1
Normal gastric tissue
GC without metastasis
GC with metastasis

j)

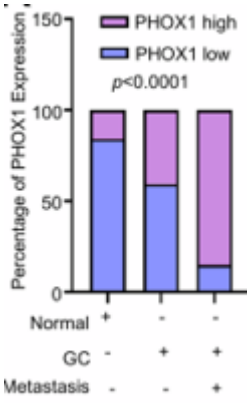
Percentage of PHOX1 Expression
PHOX1 high
PHOX1 low
p<0.0001
Normal
GC
Metastasis

k)

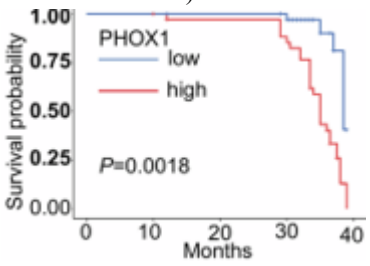
Survival probability
PHOX1
low
high
P=0.0018
Months

l)

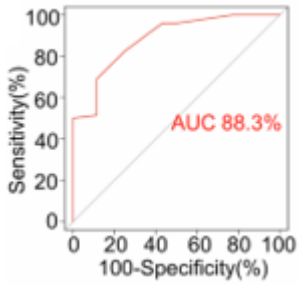
Sensitivity(%)
AUC 88.3%
100-Specificity(%)

m)

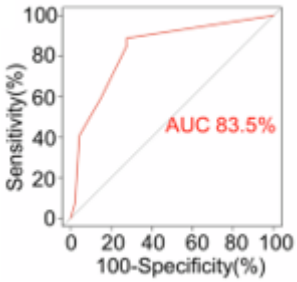

n)

Figure 1. Elevated PHOX1 Expression Predicts Poor Outcomes in Gastric Cancer

a Venn diagram displays the shared differentially expressed genes (DEGs) between gastric cancer (GC) and normal gastric tissues across four GEO datasets (GSE54129, GSE79973, GSE118916, GSE19826). **b** The partial likelihood deviance in LASSO regression is plotted, with log(λ) on the x-axis and deviance on the y-axis, based on TCGA_STAD data. **c** Coefficient profiles of PHOX1, GKN1, SOSTDC1, PGC, FUT9, GKN2, ATP4B, TFF2, and VSIG1 versus log(λ) in the LASSO model using TCGA_STAD. **d** Prognostic signature derived from DEGs for predicting patient outcomes in TCGA_STAD. **e** Comparative bar plot showing PHOX1 levels in GC tissues versus matched normal gastric mucosa in TCGA_STAD. **f** Kaplan–Meier survival analysis stratified by PHOX1 expression in TCGA_STAD. **g** ROC curve evaluating the diagnostic potential of PHOX1 in GC in TCGA_STAD. **h** RT-qPCR measurement of PHOX1 mRNA in 38 paired GC and adjacent normal tissues, normalized to GAPDH. **i** Comparison of PHOX1 mRNA in metastatic (n=31) versus non-metastatic (n=7) GC tissues, including both lymph node and distant metastases. **j** Immunohistochemical staining of PHOX1 protein in GC tissues; scale bar = 50 μm. **k** Proportion of GC samples with high or low PHOX1 expression, stratified by metastatic status. **l** Kaplan–Meier survival curves for patients grouped by optimal PHOX1 cut-off (n[low]=39, n[high]=35). M ROC curve assessing PHOX1 for discriminating GC from normal mucosa. N ROC analysis for PHOX1 distinguishing metastatic versus non-metastatic GC. P-values calculated using t-tests; *P<0.05.

Pan-cancer profiling via SangerBox (http://sangerbox.com/) revealed that PHOX1 exhibits heterogeneous expression across cancers, being significantly upregulated in 12 tumor types including GC, but downregulated in 5 others, indicating it may function as either an oncogene or tumor suppressor depending on the context. In TCGA_STAD, GC tissues showed substantially higher PHOX1 expression relative to paired normal tissues **(Figure 1e)**, and elevated PHOX1 levels were linked to shorter overall survival **(Figure 1f)**. ROC analysis produced an AUC of 0.756, suggesting PHOX1 could serve as a diagnostic biomarker **(Figure 1g)**. Clinicopathological analyses showed PHOX1 expression increases with tumor depth (T stage), metastatic progression, and overall pathological stage, while no significant associations were observed with lymph node stage, age, or sex.

Validation using our institutional cohort confirmed significantly higher PHOX1 in GC tissues compared with adjacent normal mucosa **(Figure 1h)**, with further elevation in metastatic samples **(Figure 1i)**. IHC staining revealed stronger nuclear PHOX1 expression in GC, particularly within metastatic lesions **(Figures 1j–1k)**. Stratifying patients by the optimal PHOX1 expression cut-off indicated that high PHOX1 levels correlated with poorer overall survival **(Figure 1l)**. ROC analyses further confirmed PHOX1's diagnostic potential for distinguishing tumor from normal tissue and metastatic from non-metastatic GC **(Figures 1m and 1n)**, supporting its prognostic relevance.

PHOX1 upregulation in GC is mediated by promoter hypomethylation

To investigate the epigenetic regulation of PHOX1, TCGA_STAD data revealed a significant inverse correlation between promoter methylation and mRNA levels (Spearman r = −0.2917, P<0.0001; **(Figure 2a)**). Analysis of the PHOX1 promoter region (−3000 to +500 bp from TSS) using MethPrimer (https://methprimer.com/) identified two CpG islands and multiple CpG sites. Further computational analysis with SMART_App (https://bio.tools/SMART_App) detected six CpG sites (cg03760589, cg15711902, cg23089825, cg04123776, cg07149609, cg09408098) exhibiting strong negative correlations with PHOX1 expression **(Figures 2b)**. In the GSE164988 cohort (12 matched tumor-normal pairs), cg23089825 and cg04123776 showed significant hypomethylation in tumor tissues. Survival analyses indicated that hypomethylation at cg04123776 and cg09408098 predicted worse overall survival **(Figures 2c)**, with

cg04123776 emerging as the most clinically relevant site due to its strong inverse correlation with expression, prominent hypomethylation in tumors, and prognostic value. These findings suggest that cg04123776 hypomethylation may be a key mechanism driving PHOX1 overexpression in GC.

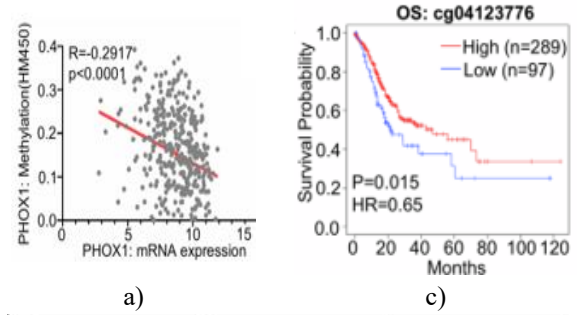

a) c)

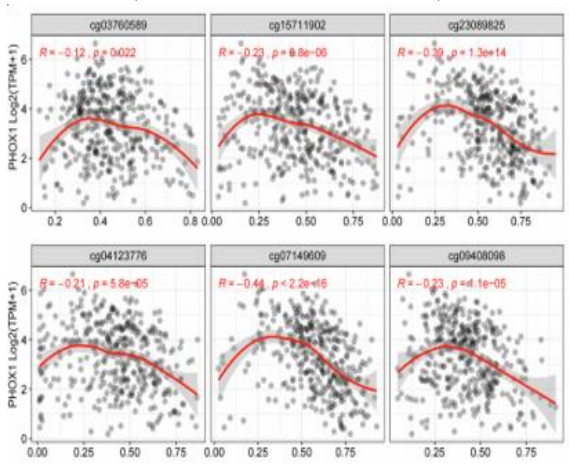

b)

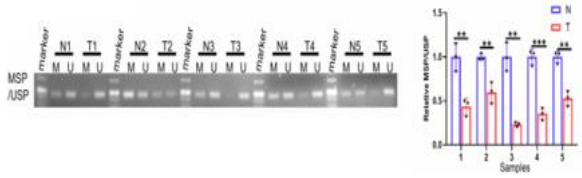

d)

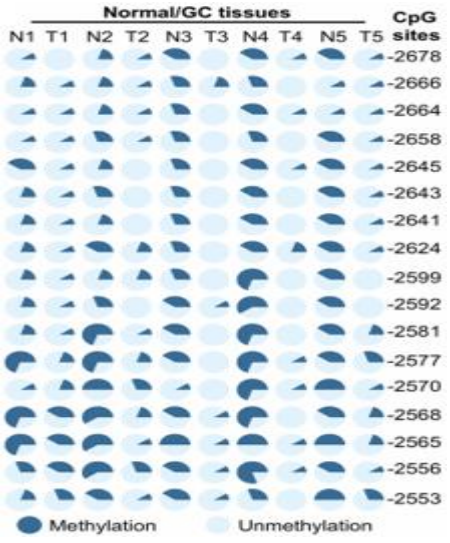

f)

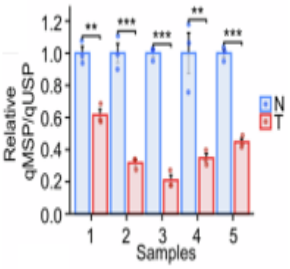

e)

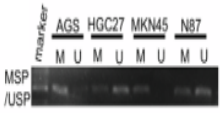

h)

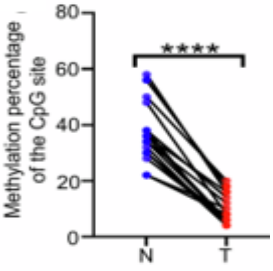

g)

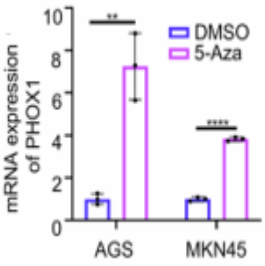

i)

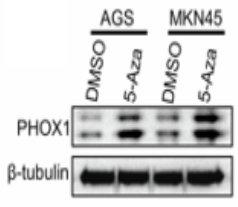

j)

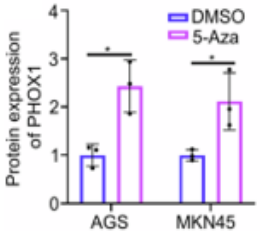

k)

Figure 2. DNA Hypomethylation Drives PHOX1 Overexpression in Gastric Cancer

a Correlation between PHOX1 mRNA levels and promoter methylation in TCGA_STAD. **b** Analysis of PHOX1 expression relative to associated CpG

sites using the SMART App. **c** Kaplan–Meier curves showing overall survival according to cg04123776 methylation status in TCGA_STAD. **d** Representative MSP gel images from five matched GC and normal tissue pairs, using primers specific for methylated (M) or unmethylated (U) alleles (left panel); band intensities were quantified and normalized to adjacent normal tissues (right panel). **e** Bar graph depicting relative methylation levels (qMSP/qUSP) of the PHOX1 promoter in paired GC (T) and normal (N) tissues. **f** Pie charts and **G** line graphs illustrating methylation patterns across the targeted PHOX1 promoter region (−2716 to −2543 bp, including cg04123776) in GC and adjacent normal mucosa; gray-blue indicates unmethylated, navy-blue methylated CpGs. **h** MSP/USP analysis of PHOX1 promoter methylation in GC cell lines. **i–k** PHOX1 mRNA and protein levels in AGS and MKN45 cells treated with or without the DNA methyltransferase inhibitor 5-aza-2′-deoxycytidine (5-Aza). P-values were determined by t-test: *P < 0.05, **P < 0.01, ***P < 0.001, ****P < 0.0001.

To assess the functional impact of cg04123776 hypomethylation on PHOX1 expression, we performed targeted methylation analysis in randomly selected matched tumor-normal tissue pairs (−2706 to −2533 bp relative to TSS). Initial qualitative MSP and USP analyses confirmed differential methylation between GC and normal tissues, with tumors exhibiting reduced methylated PHOX1 promoter signals **(Figure 2d)**. Quantitative methylation-specific PCR (qMSP) further validated these results, showing a significantly lower fraction of methylated alleles in tumor tissues relative to matched normal mucosa **(Figure 2e)**. Bisulfite sequencing (BSP) revealed pronounced hypomethylation of the PHOX1 promoter in tumor tissues **(Figures 2f and 2g)**. In line with clinical observations, PHOX1-high GC cell lines (HGC27, N87) exhibited notable promoter hypomethylation, whereas PHOX1-low lines (AGS, MKN45) maintained higher methylation levels **(Figure 2h)**. Treating AGS and MKN45 cells with 5-Aza, a DNA methyltransferase inhibitor, led to upregulation of both PHOX1 mRNA and protein, demonstrating that promoter hypomethylation directly regulates PHOX1 expression **(Figures 2i–2k)**. These data establish that DNA hypomethylation at cg04123776 is a key mechanism driving PHOX1 overexpression in GC.

PHOX1 enhances GC cell proliferation and motility in vitro

To explore the oncogenic function of PHOX1, we first profiled its expression across GC cell lines. Western blot and RT-qPCR analyses indicated lower PHOX1 levels in AGS and MKN45 cells compared to HGC27 and N87. We then generated isogenic models: AGS_PHOX1 and MKN45_PHOX1 cells stably overexpressing PHOX1, and HGC27_shPHOX1 and N87_shPHOX1 cells with PHOX1 knockdown. Functional assays revealed that PHOX1 overexpression significantly promoted cell proliferation and colony formation in AGS and MKN45, whereas knockdown suppressed growth in HGC27 and N87 **(Figures 3a–3d)**. Transwell migration and invasion assays further demonstrated that PHOX1 upregulation enhances motility and invasiveness, while PHOX1 depletion reduces these properties **(Figures 3e–3h)**. Collectively, these results indicate that PHOX1 strongly drives GC cell proliferation, migration, and invasion.

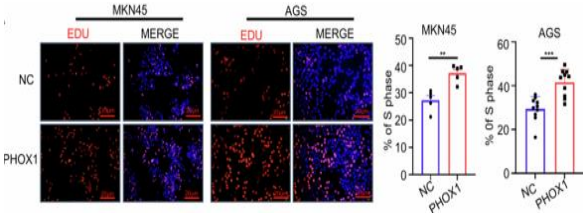

a)

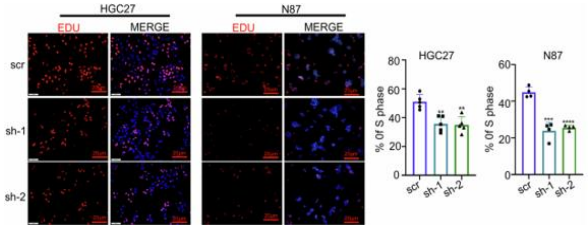

b)

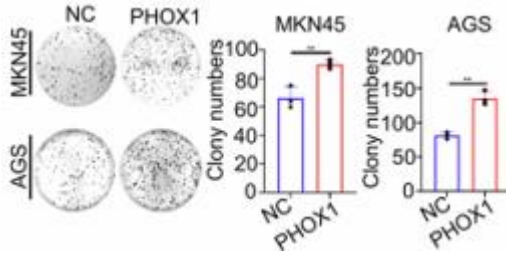

c)

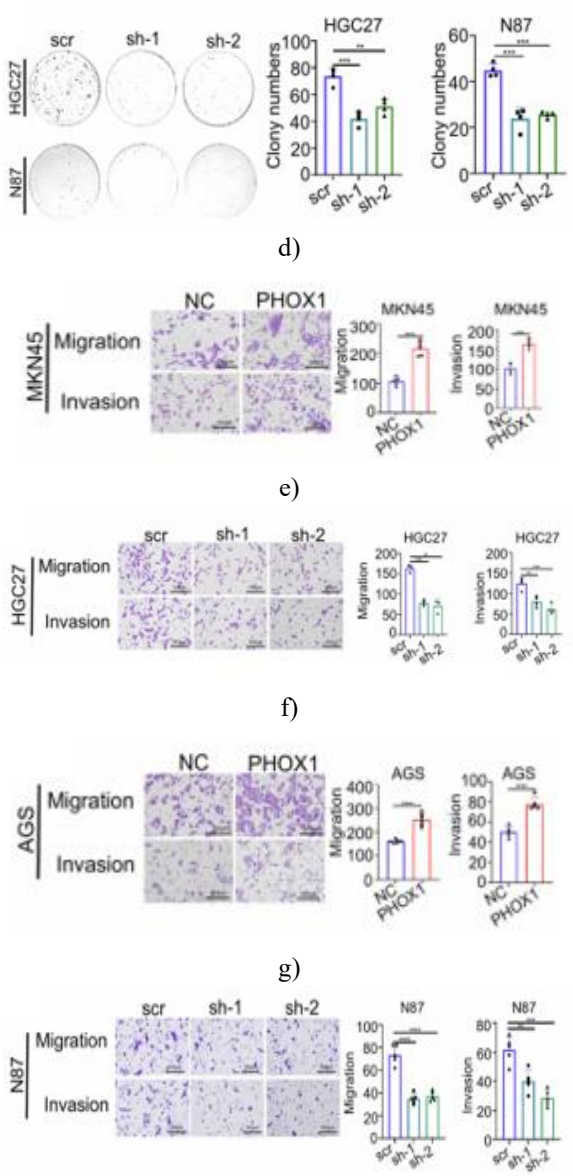

Figure 3. PHOX1 drives proliferation and motility of GC cells in vitro.

a, b EdU incorporation assays demonstrate changes in GC cell proliferation upon PHOX1 overexpression or silencing (**a, b**). Scale bar: 20 μm. **c, d** Colony formation assays display representative images and the corresponding quantification of colony numbers in GC cells with altered PHOX1 levels. e–h Migration and invasion assays show representative micrographs and quantified results. Statistical analysis was performed using a t-test: $^{**}P < 0.01$, $^{***}P < 0.001$, $^{****}P < 0.0001$.

PHOX1 enhances tumor growth and metastatic potential of GC cells in vivo

To investigate PHOX1's oncogenic effects in vivo, GC cells with either elevated or reduced PHOX1 expression were implanted in multiple xenograft models. Subcutaneous tumors derived from PHOX1-overexpressing cells grew substantially faster than control tumors **(Figures 4a–4c)**. Histopathological evaluation through H&E and Ki-67 staining further confirmed markedly higher proliferation rates in tumors with PHOX1 upregulation **(Figure 4d)**.

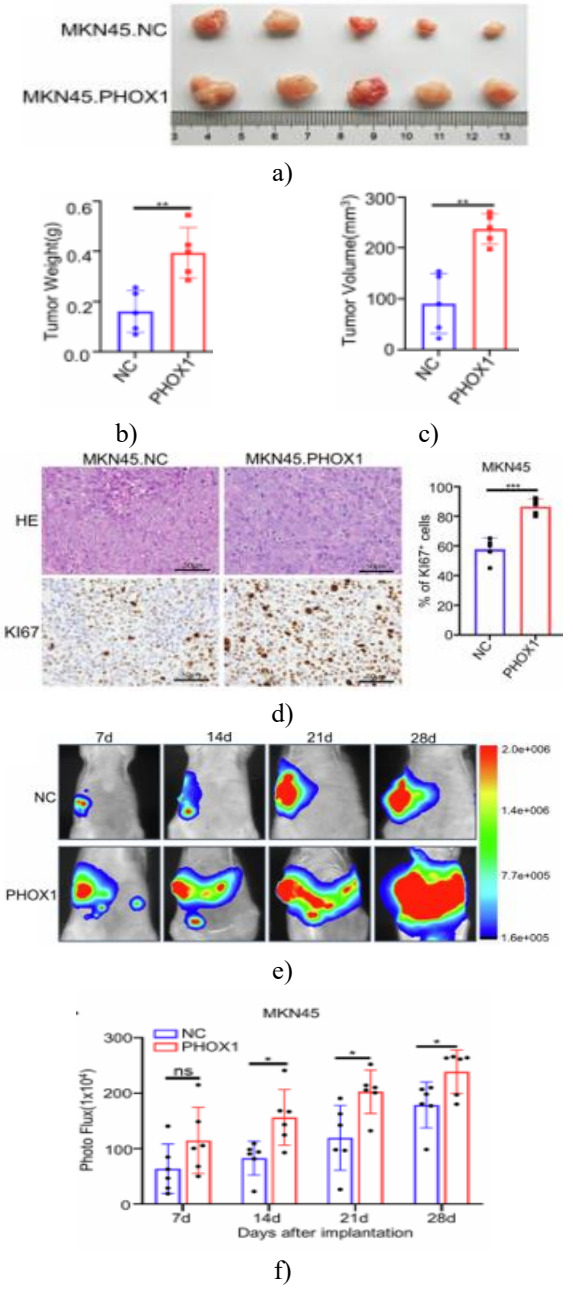

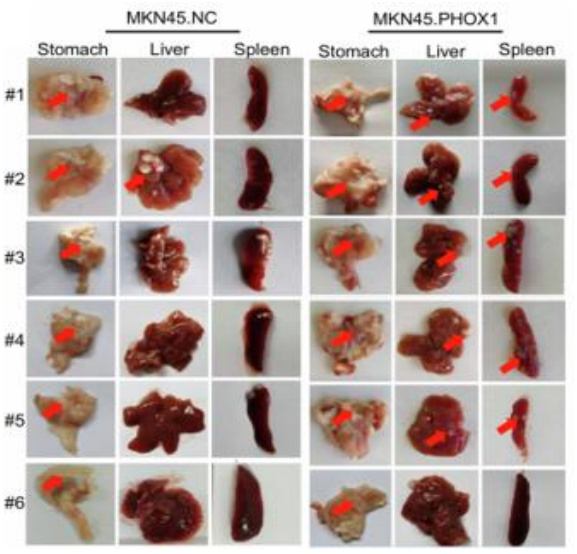

g)

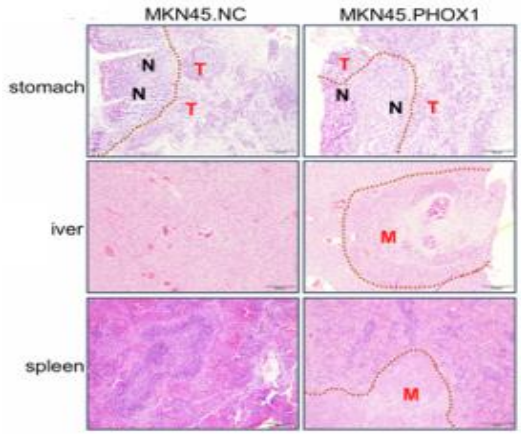

h)

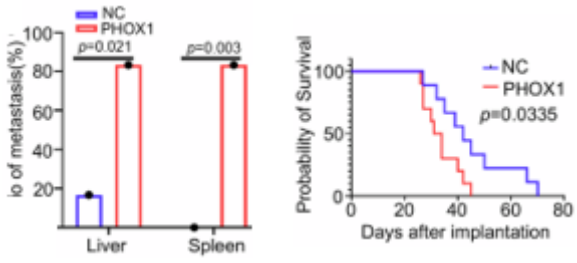

i) j)

Figure 4. PHOX1 drives tumor growth and metastatic spread of GC cells in vivo. **a** Representative images show subcutaneous tumors generated from GC cells engineered to overexpress PHOX1 (n = 5 per group). **b and c** Tumor weight and volume measurements confirm that PHOX1-overexpressing tumors are significantly larger than controls (n = 5). **d** Histological analyses using H&E and Ki-67 immunostaining reveal enhanced cellular proliferation in PHOX1-high tumors. Scale bars: 50 μm. **e** Bioluminescence imaging of MKN45-Luc xenografts implanted orthotopically into mouse stomachs demonstrates increased signal intensity in the PHOX1-overexpressing group. **f** Quantification of fluorescence signals highlights elevated tumor burden in these mice. **g** Macroscopic images of orthotopic GC tumors, livers, and spleens indicate larger primary tumors and more visible metastases in PHOX1-overexpressing animals. **h** H&E staining of these tissues confirms extensive metastatic involvement. Scale bars: 100 μm. **i** Liver and spleen metastasis rates were quantified, showing a significant increase in the PHOX1 group, with significance determined by chi-square test. **j** Survival analysis using Kaplan–Meier curves demonstrates that mice bearing PHOX1-overexpressing tumors had markedly reduced overall survival (n = 6 per group). *P < 0.05, **P < 0.01, ***P < 0.001, ns, not significant.

In the orthotopic model with luciferase-labeled MKN45 cells, overexpression of PHOX1 markedly enhanced bioluminescence signals and resulted in a higher number of metastatic foci compared with control tumors **(Figures 4e and 4f)**. Examination of primary tumors and metastatic organs showed that PHOX1-overexpressing tumors were not only larger but also displayed more aggressive histological features, with a higher incidence of liver and spleen metastases **(Figures 4g–4i)**. Consistent with these findings, mice implanted with PHOX1-overexpressing cells exhibited significantly shorter survival compared with controls **(Figure 4j)**, indicating that PHOX1 promotes both tumor growth and metastatic dissemination in vivo.

PHOX1 transcriptionally induces NGFR expression

To explore the mechanism underlying PHOX1-driven GC progression, RNA-seq was performed on AGS cells with PHOX1 overexpression. Differential gene expression analysis (fold change ≥ 2) identified 2084 genes upregulated and 194 downregulated. Screening of the top 50 upregulated genes **(Figures 5a and 5b)** and correlation analysis in the TCGA_STAD dataset revealed 11 candidate genes showing a significant positive correlation with PHOX1 (Spearman r > 0.5, p < 0.05), including TMEM119, SHANK1, LRRC15, DACT3, OLFML3, FOXS1, CHST1, NOVA2, SCN2B, NGFR, and CYTH4 **(Figure 5c)**. Among these, NGFR consistently displayed the highest upregulation

(log2FC > 2) across multiple GC cell lines (AGS, MKN45, HGC27, N87) upon PHOX1 modulation **(Figures 5d)**, identifying NGFR as a principal downstream target of PHOX1 in gastric cancer.

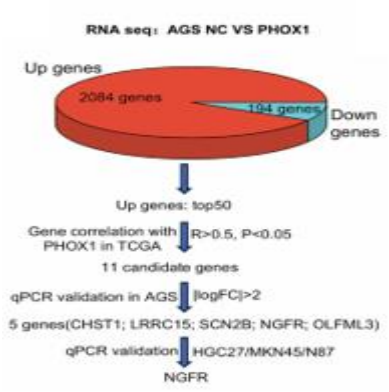

a)

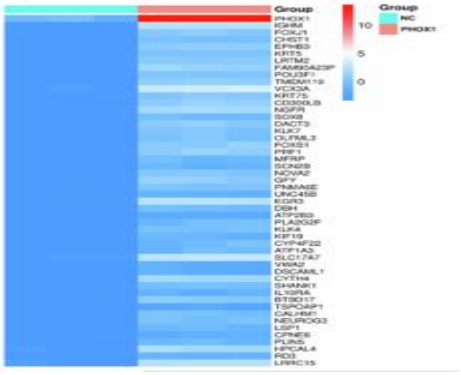

b)

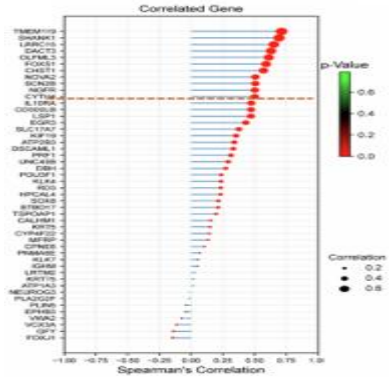

c)

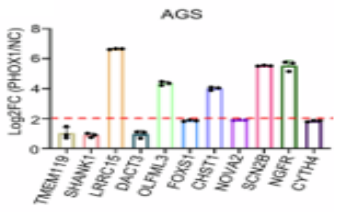

d)

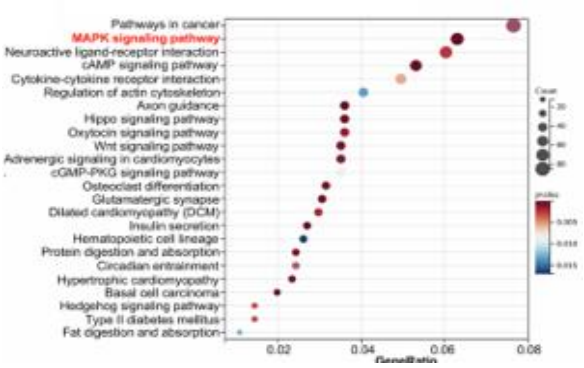

e)

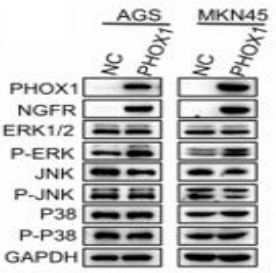

f)

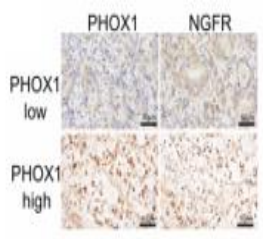

g)

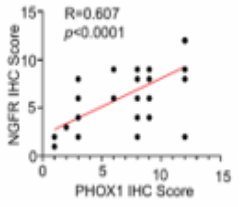

h)

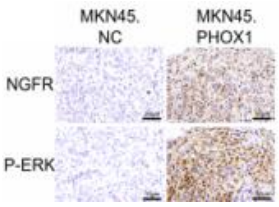

i)

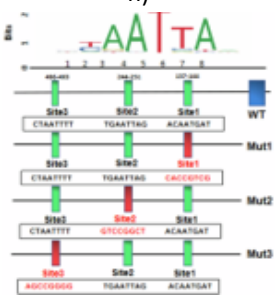

j)

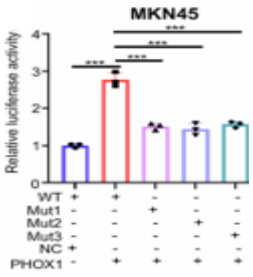

k)

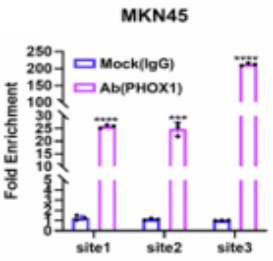

l)

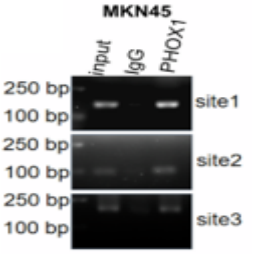

m)

Figure 5. PHOX1 drives NGFR expression and activates ERK1/2 signaling in gastric cancer.

a Overview of the experimental approach used to pinpoint downstream targets of PHOX1 in AGS cells. **b** Heatmap showing the 50 genes most strongly upregulated after PHOX1 overexpression. **c** Correlation analysis of these top 50 genes with PHOX1 expression in TCGA_STAD samples. **d** RT-qPCR validation of candidate DEGs affected by PHOX1 overexpression. **e** KEGG pathway enrichment analysis of DEGs visualized as a bubble plot, highlighting signaling pathways altered by PHOX1. **f** Western blot analysis confirming NGFR upregulation and ERK1/2 activation in PHOX1-overexpressing cells. **g, h** Representative IHC images of PHOX1 and NGFR expression in GC patient tissues (G) and their statistical correlation across 62 samples (H). **i** IHC images of NGFR and phosphorylated ERK (P-ERK) in mouse orthotopic GC tumors. **j** Predicted PHOX1 binding sites on the NGFR promoter identified using the JASPAR database. **k** Luciferase reporter assays testing transcriptional activation of WT or mutant NGFR promoters by PHOX1 in GC cell lines. **l, m** ChIP-qPCR and agarose gel electrophoresis showing PHOX1 binding to three NGFR promoter sites. Significance: *P < 0.05; **P < 0.01; ***P < 0.001; ****P < 0.0001; ns, not significant.

KEGG analysis of RNA-seq data indicated that MAPK signaling is a principal pathway downstream of NGFR **(Figure 5e)**. Consistently, western blot confirmed that PHOX1 overexpression elevated NGFR levels and increased ERK1/2 phosphorylation, suggesting activation of the MAPK cascade **(Figure 5f)**. Further computational analysis using GEPIA2 revealed a strong positive correlation between PHOX1 and NGFR in STAD patient samples. In line with this, IHC and RT-qPCR demonstrated higher NGFR expression in GC tissues exhibiting elevated PHOX1, with high NGFR levels associated with poorer patient prognosis **(Figures 5g and 5h)**. In vivo, orthotopic xenograft tumors overexpressing PHOX1 showed pronounced NGFR and P-ERK upregulation **(Figure 5i)**, supporting the hypothesis that PHOX1 modulates NGFR-ERK1/2 signaling.

Because PHOX1 is a transcription factor, we explored whether it directly controls NGFR transcription. JASPAR predictions revealed three potential PHOX1-binding motifs in the NGFR promoter **(Figure 5j)**. Luciferase assays confirmed that PHOX1 activated transcription at all three sites in AGS and MKN45 cells **(Figures 5k)**. ChIP-qPCR further verified PHOX1 occupancy at these promoter regions **(Figures 5l and 5m)**, establishing NGFR as a direct transcriptional target.

PHOX1 enhances GC cell proliferation and migration via NGFR-ERK1/2 signaling

To clarify the functional importance of NGFR-ERK1/2 in PHOX1-mediated GC progression, rescue experiments were performed using NGFR-targeted siRNA and the ERK1/2 inhibitor SCH772984 (ERKi). Knockdown efficiency was validated by RT-qPCR and western blotting **(Figures 6a–6d)**. Suppressing NGFR significantly reduced the proliferative and migratory advantages conferred by PHOX1 overexpression **(Figures 6e–6g)**. Similarly, ERK1/2 inhibition curtailed proliferation and motility in PHOX1-overexpressing cells **(Figures 6h–6k)**. Western blot analysis revealed that both NGFR silencing and ERK inhibition markedly diminished PHOX1-driven upregulation of p-ERK, MMP1, CCND1, VEGFA, and FOS, all critical effectors of tumor growth and metastasis in GC [19, 20] **(Figures 6l–6o)**. Collectively, these results demonstrate that the NGFR-ERK1/2 axis is a key mediator of PHOX1-induced gastric cancer progression.

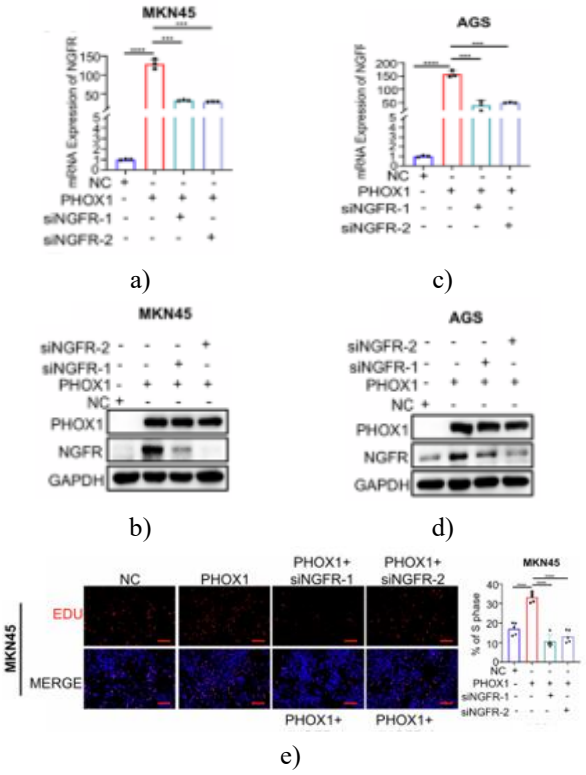

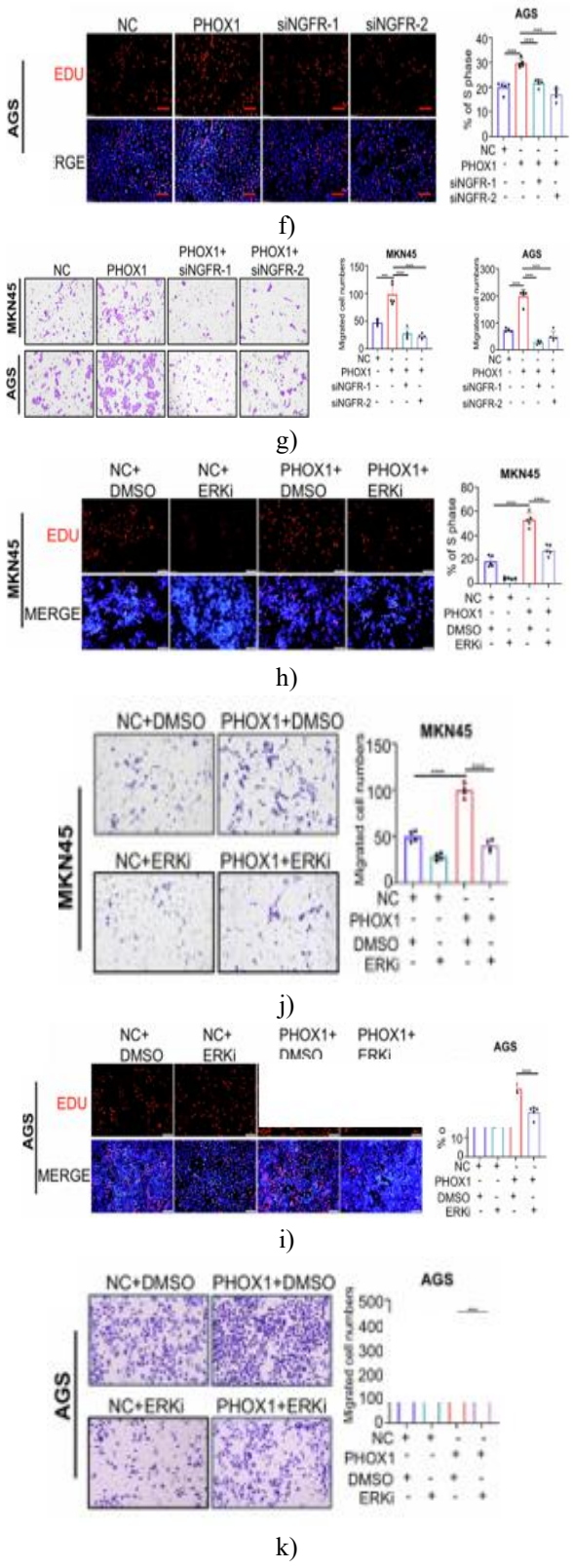

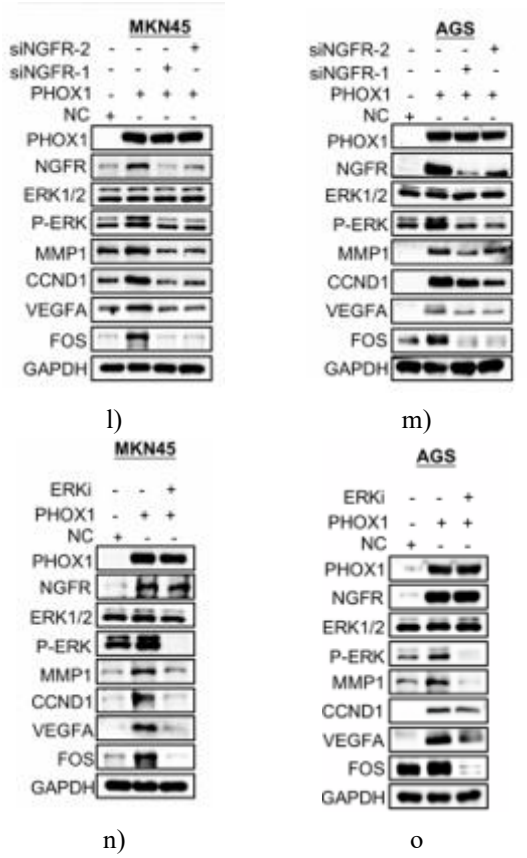

Figure 6. PHOX1 drives GC cell proliferation and migration via the NGFR-ERK1/2 signaling axis. **a–d** Successful establishment of GC cell models overexpressing PHOX1 or with NGFR knockdown was confirmed 48 hours post-transfection using RT-qPCR and western blot assays. **e, f** EdU incorporation assays revealed that silencing NGFR significantly reduced the proliferation of PHOX1-overexpressing GC cells. **g** Transwell migration assays demonstrated that NGFR knockdown impaired the migratory capacity of PHOX1-overexpressing cells. **h, i** Treatment with the ERK1/2 inhibitor SCH772984 (ERKi) markedly suppressed proliferation in PHOX1-overexpressing GC cells, as measured by EdU assay. **j, k** Transwell assays indicated that ERK1/2 inhibition also substantially curtailed cell migration. **l–o** Western blot analysis showed that both NGFR depletion and ERKi treatment attenuated the PHOX1-driven upregulation of key ERK1/2 pathway effectors, including p-ERK, MMP1, CCND1, VEGFA, and FOS. Statistical significance: ***P < 0.001, ****P < 0.0001.

Our findings establish PHOX1 as a pivotal oncogenic driver in gastric cancer, functioning through a previously uncharacterized epigenetic-transcriptional signaling cascade. By combining multi-cohort data analysis with functional experiments, we have uncovered the PHOX1-NGFR-ERK1/2 axis as a critical mediator of GC aggressiveness, with clear associations to poor clinical outcomes. This work expands the current understanding of GC biology and identifies potential therapeutic targets. While PHOX1's oncogenic role has been reported in several cancers [13, 21–26], its relevance in GC remained largely unexplored. Through comprehensive evaluation of GEO, TCGA, and institutional patient samples, we consistently observed elevated PHOX1 expression in GC tissues, which correlated strongly with advanced tumor stage and reduced survival. Although TWIST1 has been implicated in PHOX1 regulation in renal fibrosis [27], regulatory mechanisms in cancer have been poorly defined. Here, we reveal that promoter hypomethylation at CpG site cg04123776 is a primary mechanism driving PHOX1 overexpression in GC. The causal link between DNA demethylation and PHOX1 upregulation was confirmed via 5-aza-2′-deoxycytidine treatment. Clinically, PHOX1 hypomethylation also correlated with unfavorable prognosis, highlighting its potential as a prognostic marker. Limitations include the modest size of our clinical validation cohort and the need to further elucidate how cg04123776 hypomethylation mechanistically enhances PHOX1 transcription.

Functional assays demonstrated that PHOX1 promotes GC cell proliferation and migration both in vitro and in vivo. RNA-seq and follow-up validation identified NGFR as a key downstream target of PHOX1. NGFR is a transmembrane receptor known to activate ERK1/2 signaling and support tumor progression [28–31]. Our data indicate that PHOX1 drives NGFR expression, which in turn stimulates ERK1/2 phosphorylation—a central oncogenic pathway in cancer [20]. Importantly, disrupting NGFR expression or inhibiting ERK1/2 signaling effectively counteracted PHOX1-driven proliferation and motility, confirming the functional relevance of the PHOX1-NGFR-ERK1/2 axis. These results align with extensive literature documenting the role of sustained ERK1/2 activation in cancer progression [32–36].

The PHOX1-NGFR-ERK1/2 pathway also presents clinically actionable opportunities. First, PHOX1 promoter methylation status at cg04123776 could serve as a biomarker for patient stratification and prognosis. Second, therapeutic interventions targeting this axis—either by silencing NGFR or pharmacologically inhibiting ERK1/2—demonstrated substantial inhibition of PHOX1-mediated oncogenic effects, highlighting a potential treatment strategy.

In summary, this study delineates a complete oncogenic pathway in GC, linking epigenetic alterations to transcriptional regulation and downstream kinase signaling. The identification of the PHOX1-NGFR-ERK1/2 axis not only enriches our understanding of GC pathophysiology but also provides a foundation for the development of targeted therapeutic strategies against this aggressive malignancy.

Materials and Methods

Patient specimens and cell maintenance

Human gastric cancer (GC) tissues (n=74) along with matched non-cancerous gastric tissues (n=44) were collected from individuals undergoing surgery at Guangdong Provincial People's Hospital. No patient had received neoadjuvant chemotherapy or radiotherapy. The study protocol was approved by the hospital's ethics committee, and all participants gave informed consent in writing.

Cell lines investigated comprised the immortalized gastric epithelial line GES-1 and GC lines AGS, MGC803, N87, MKN45, and HGC27, plus HEK293T for viral packaging. All were sourced from the Chinese Academy of Medical Sciences Cell Bank (Shanghai, China). Cultures of GES-1, AGS, MGC803, N87, and MKN45 utilized RPMI-1640 base medium, whereas HGC27 and HEK293T were grown in DMEM base medium. Each was fortified with 10% fetal bovine serum (FBS; Sigma-Aldrich, USA; cat. no. F0193). Incubation occurred under standard conditions (37°C, 5% CO_2, humidified).

To rule out contamination, routine mycoplasma screening was conducted on every line using the Myco-Lumi™ Luminescent Detection Kit (Beyotime Biotechnology, cat. no. C0298S), adhering precisely to the supplied protocol. All tests returned negative.

Analysis of TCGA dataset and survival correlation

Public TCGA gastric cancer data were interrogated through the Xiantao web tool, which offers integrated pipelines for omics analysis and clinical correlations.

Overall survival (OS) was evaluated via the platform's survival module. Cases were dichotomized into elevated

or reduced PHOX1 expression cohorts using the algorithm-determined optimal threshold. Kaplan–Meier plots depicted OS differences, with significance tested by log-rank method ($P < 0.05$ indicating relevance).

Plasmid construction for gene modulation, viral packaging, and stable line generation

PHOX1-directed shRNAs were synthesized and incorporated into the puromycin-resistant lentiviral backbone pLVX-puro (Geneyuan Co., Ltd., Guangzhou, China). Sequences included shRNA-1 (5′-GGAATAGGACAACCTTCAA-3′), shRNA-2 (5′-CACGTGACACGTTCGGAGA-3′), and scrambled control shNC (5′-TTCTCCGAACGTGTCACGT-3′).

For gain-of-function studies, the PHOX1 open reading frame was cloned into pLVX-3×FLAG-Puro (Geneyuan Co., Ltd.) employing Clone Enzyme Mix (Thermo Fisher Scientific, USA), resulting in pLVX-PHOX1-3×FLAG.

Lentiviral particles were generated by transfecting HEK293T cells with the transfer vector plus helper plasmids psPAX2 and pMD2.G (4:3:1 mass ratio) using Lipofectamine 2000 (Invitrogen, USA). Medium was exchanged 12 hours later. Supernatant harvested at 60 hours post-transfection was centrifuged (3000 rpm, 4°C, 10 min) to remove debris and filtered (0.45 μm PVDF; JET BIOFIL, cat. no. FPE404000). Aliquots were frozen at −80°C.

GC cells were transduced with virus supplemented with 8 μg/mL polybrene (Beyotime, cat. no. ST1380) for 24 hours, followed by recovery in complete medium. Stable integrants were enriched by 72-hour exposure to 2 μg/mL puromycin. Appropriate controls were pLVX-3×FLAG-luci-Puro (overexpression) and pLVX-shNC-puro (knockdown).

NGFR silencing via transient siRNA

NGFR-specific siRNAs were developed targeting human NGFR transcript (NM_002507.4) via Santa Cruz's design tool and produced by Geneyuan Co., Ltd. (Guangzhou, China) with desalting purification. Sequences: siNGFR-1 (5′-GACAAGCAGAACACCGTGT-3′), siNGFR-2 (5′-CGTTGGATTACACGGTCCA-3′). Specificity was verified by BLAST. A non-specific control si-NC (5′-TTCTCCGAACGTGTCACGT-3′) was included.

Transfection into GC lines (e.g., AGS, MKN45) employed 100 nM oligos and Lipofectamine 3000 (Invitrogen, USA) per instructions. Efficacy of target depletion was assessed 48 hours later by RT-qPCR and immunoblotting.

RNA preparation and quantitative PCR

Cellular or tissue RNA was purified with TRIzol reagent (Invitrogen, USA). First-strand cDNA synthesis used the Evo M-MLV RT Kit for qPCR (Accurate Biology, cat. no. AG11706). Amplification relied on SYBR Green Pro Taq HS Premix (Accurate Biology, cat. no. AG11718) run on a LightCycler 480 II (Roche). Expression was normalized to GAPDH and quantified by the $2^{-\Delta\Delta Ct}$ approach.

Immunohistochemistry (IHC)

Tissue sections embedded in paraffin were analyzed using an IHC kit (ZSGB Bio, China) according to the supplied protocol. Sections were incubated overnight at 4 °C with primary antibodies: anti-PHOX1 (1:500; Abcam, Cat. No.: ab211292), anti-NGFR (1:500; Bioss Antibodies, Cat. No.: bs-7122R), anti-p-ERK (1:500; Cell Signaling Technology, Cat. No.: 4370S, USA), and anti-Ki67 (1:10,000; Huabio Technology, Cat. No.: HA721115, China). The staining intensity was classified as 0 (negative), 1 (weak), 2 (moderate), or 3 (strong), and the proportion of positive cells was graded as 0 (<5%), 1 (5–25%), 2 (26–50%), 3 (51–75%), or 4 (76–100%). Final scores were calculated by multiplying the intensity and proportion values. Two pathologists, blinded to the sample identities, scored the slides independently, and the mean value was used for each specimen.

Methylation analysis: MSP, USP, qMSP, qUSP, and BSP

Genomic DNA from gastric cancer tissues and cell lines was isolated using the DNA Extraction Kit (Tiangen Biotech, Cat. No.: DP304, China). For methylation studies, 500 ng of DNA underwent bisulfite conversion using the EZ DNA Methylation Kit (Zymo Research, Cat. No.: D5001, USA) as per the manufacturer's instructions. Conventional MSP and USP were performed in 50 μl reactions with PerfectStart Taq DNA Polymerase (TransGen Biotech, Cat. No.: AP401, Beijing, China), and products were resolved on 2% agarose gels stained with GoldView (Accurate Biology, Cat. No.: AG11915, China).

Reactions included an initial denaturation at 95 °C for 10 min, followed by 40 cycles at 95 °C for 15 s and 60 °C for 1 min (annealing/extension). The β-actin gene, targeting a CpG-poor region to avoid methylation bias, served as an internal reference (forward: 5′-GGGTGGTGATGGAGGAGGTT-3′; reverse: 5′-TAACCACCACCCAACACACAAT-3′) [37]. Experiments were performed in triplicate. Relative

methylation and unmethylation levels were determined using the $2^{-\Delta\Delta Ct}$ method, where ΔCt = Ct(PHOX1) − Ct(β-actin) and ΔΔCt = ΔCt(sample) − ΔCt(control). Results are expressed as mean ± SD from three independent experiments.

For bisulfite sequencing (BSP), converted DNA fragments covering the PHOX1 CpG island were amplified using MethPrimer 2.0-designed primers and the PerfectStart Taq DNA Polymerase Kit (TransGen Biotech, Cat. No.: AP401, China). Amplicons were purified using the DNA Gel Extraction Kit (TransGen Biotech, Cat. No.: DP209, Beijing, China), ligated into a T-vector, and transformed into DH5α competent E. coli. Ten clones per sample were cultured in LB medium at 37 °C with shaking at 200 rpm. Plasmids were isolated with the TIANprep Plasmid Mini Kit (Tiangen Biotech, Cat. No.: DP118, China) and sequenced using M13 primers (Applied Biosystems, Waltham, MA, USA).

Western blot (WB)

Protein extracts were separated on SDS-PAGE gels and transferred to PVDF membranes. Membranes were incubated with primary antibodies overnight at 4 °C, washed thrice with TBST (10 min each), and then probed for 1 h at 22–25 °C with HRP-conjugated secondary antibodies: Goat Anti-Mouse IgG H&L/HRP (1:10,000; Cat. No.: bs-40296G-HRP, Bioss Antibodies, China) or Goat Anti-Rabbit IgG H&L/HRP (1:10,000; Cat. No.: bs-0295G-HRP, Bioss Antibodies, China). Protein bands were visualized using Super ECL Detection Reagent (Yeasen Biotechnology, Cat. No.: 36208ES76, China) and imaged with a BLT Photon Technology Imager.

EdU incorporation assay for cell proliferation

To quantify proliferative activity in gastric cancer cells, cells were plated into 48-well culture plates at densities tailored to the experimental requirements. EdU labeling was carried out by adding 10 μM EdU to each well in 200 μl of complete medium, followed by incubation for 1 h at 37 °C in a humidified atmosphere containing 5 percent CO_2. After incorporation, cells were fixed with freshly prepared 4 percent paraformaldehyde for 30 min at room temperature to preserve cellular architecture. Permeabilization was performed using 0.5% Triton X-100 in PBS for 30 min to allow staining reagents access to nuclear DNA. Nuclei were counterstained with Hoechst 33342 for 10–15 min. Detection of incorporated EdU was conducted using the BeyoClick™ EdU-594 Kit (Beyotime Biotechnology, Cat. No.: C0078S, China) according to the kit protocol. Images were captured at ×200 magnification using a Leica fluorescence microscope (Leica Microsystems, Wetzlar, Germany), selecting five fields at random per sample, ensuring identical exposure for comparative quantification.

Colony formation assay

Cells were seeded sparsely (500 cells per well) into 6-well plates to allow individual colonies to form over 14 days under standard culture conditions (37 °C, 5 percent CO_2, 95 percent humidity). Following incubation, colonies were fixed with ice-cold methanol for fifteen minutes, stained with hematoxylin for five minutes, and colonies containing 50 or more cells were counted. Each experiment was performed with three independent biological replicates, and technical triplicates were included to ensure reproducibility.

Transwell migration and invasion

Cell migratory and invasive capacities were assessed using 8-μm pore Transwell inserts (Corning, USA). For migration, 1×10^5 cells in serum-free medium were placed in the upper chamber, whereas for invasion, inserts were first coated with Matrigel (Corning, USA) to simulate extracellular matrix barriers. The lower chambers contained medium supplemented with 10% FBS to serve as a chemoattractant. Cells were incubated under standard conditions for 24–72 h, depending on the cell line. Non-migratory or non-invaded cells were gently removed from the upper membrane, and cells that traversed the membrane were fixed with 4 percent PFA for fifteen minutes and stained with hematoxylin for five minutes. Five random microscopic fields per insert were captured for counting, and cell numbers were quantified manually.

Luciferase reporter analysis of PHOX1-regulated NGFR expression

Potential PHOX1 binding motifs within the NGFR promoter were identified using the JASPAR database (http://jaspar.genereg.net). A segment of the NGFR promoter containing three candidate binding sites was cloned into the PGL3 luciferase reporter to generate the wild-type (WT) construct. Mutant constructs (Mut1–3) were created by introducing point mutations at each predicted binding site. AGS and MKN45 cells were co-transfected with PHOX1 overexpression plasmids, PGL3 (WT or Mut1–3) constructs, and the pTK-Renilla luciferase control vector using Lipofectamine® 3000

(Thermo Fisher Scientific, USA). Forty-eight hours post-transfection, luciferase activity was measured using the Dual-Luciferase Reporter Assay System (TransDetect® Bright-Luc, TransGen Biotech, China). Firefly luciferase signals from the PGL3 vector were normalized to Renilla luciferase signals from pTK, and the activity of the WT reporter co-transfected with empty vector was defined as 1.0. Activities of other experimental groups were expressed as fold-change relative to this baseline.

Chromatin immunoprecipitation (ChIP) with qPCR validation

The interaction between PHOX1 and the NGFR promoter was assessed using the EZ-Magna ChIP® A/G Kit (Sigma-Aldrich, Cat. No.: 17-10086, USA). Cells were first treated with formaldehyde to stabilize protein-DNA complexes and then lysed to release chromatin. DNA was sheared on ice through sonication at 40–60% amplitude in cycles of 30 s on/30 s off, repeated 10–15 times, yielding fragments ranging from 200 to 1000 base pairs. Immunoprecipitation was performed overnight at 4 °C with either an anti-FLAG antibody (1:100; Proteintech, China) or control rabbit IgG. Following precipitation, DNA was eluted and de-crosslinked at 65 °C overnight, with 1% of input DNA retained as a reference.

RNA sequencing (RNA-seq)

Total RNA was isolated from AGS.NC and AGS.PHOX1 cells using TRIzol (Invitrogen), followed by DNase I treatment to eliminate contaminating genomic DNA. RNA purity and integrity were confirmed using NanoDrop 2000 (OD260/280: 1.8–2.0) and Agilent Bioanalyzer (RIN ≥ 8.0). mRNA was captured with oligo(dT) beads, and cDNA libraries were generated using the NEBNext Ultra RNA Library Prep Kit (Illumina). Libraries were sequenced on an Illumina HiSeq platform, generating 150-bp paired-end reads. Low-quality reads were removed, and clean reads were aligned to the human genome (GRCh38) using HISAT2. Gene expression levels were estimated using StringTie, and DEGs were identified through DESeq2, considering $|\log2FC| \geq 2$ and adjusted $P < 0.05$ as thresholds. Each condition included three biological replicates.

Subcutaneous xenograft models

Female BALB/c nude mice (4 weeks old, nu/nu; Guangdong Medical Laboratory Animal Center, Guangzhou, China) were housed in SPF conditions for one week before experiments. Mice were stratified by body weight and randomly assigned to groups. GC cells in exponential growth (1×10^6 cells/100 µl) were injected subcutaneously into the dorsal flank (n = 5 per group). Tumor dimensions were measured for 20 days, and volumes were calculated as (length × width²)/2. Investigators performing measurements were blinded to group assignments, and mice succumbing to injection-related complications were excluded. Tumors were collected post-mortem, weighed, and fixed in 4% PFA at 4 °C for 24 h before paraffin embedding for histology.

Orthotopic gastric cancer models

Orthotopic tumors were established in 4-week-old female BALB/c nude mice according to established protocols [38]. Mice were anesthetized with ketamine (70 mg/kg), a small incision was made to expose the stomach, and 1×10^6 GC cells in 100 µl were injected into the muscular layer. To prevent infection, penicillin-streptomycin (100 U/ml and 100 µg/ml, respectively) was administered, and the incision was sutured. Mice were monitored for two months and euthanized upon signs of cachexia. Tumors were harvested and fixed for subsequent analyses.

Epigenetic demethylation with 5-Aza-2'-deoxycytidine

To investigate the effect of DNA demethylation on PHOX1 expression, GC cells in active proliferation were plated in 60-mm dishes and cultured overnight to achieve 30–50% confluency. Cells were then continuously exposed to 5 µM 5-azacytidine (5-Aza; Sigma-Aldrich, Cat. No.: 189825, USA; dissolved in DMSO) under standard culture conditions (37 °C, 5% CO_2) for three consecutive days, with the medium refreshed every 24 hours to maintain drug potency. Following this treatment, cells were collected to evaluate changes in PHOX1 at both the transcript and protein levels.

Inhibition of ERK signaling using SCH772984

To assess the role of ERK signaling, cells were seeded into 60-mm dishes and allowed to adhere overnight. The following day, cells were treated with 5 µM SCH772984 (MedChemExpress, Cat. No.: HY-50846, USA; dissolved in DMSO) for 24 hours, while control cells received an equivalent volume of DMSO. All experiments were conducted in triplicate to ensure reproducibility and reliability of the results.

Data analysis and statistical methods

Quantitative data were analyzed using SPSS 22.0 and GraphPad Prism 9.0. Unless otherwise specified, all experiments included at least three biological replicates, each performed with three technical repeats. Two-group comparisons were assessed using two-tailed Student's t-tests (paired or unpaired depending on sample dependency). Categorical variables were examined using the Chi-square test. For analyses involving three or more experimental groups, one-way or two-way ANOVA was employed, with data normality verified using the Shapiro–Wilk test before parametric testing. Post hoc pairwise comparisons following ANOVA were corrected with the Benjamini–Hochberg method to control the false discovery rate. Kaplan–Meier survival curves were generated to estimate overall survival (OS), and statistical significance between survival curves was determined using the log-rank test.

Acknowledgments: None

Conflict of Interest: None

Financial Support: None

Ethics Statement: None

References

1. Thrift AP, El-Serag HB. Burden of gastric cancer. Clin Gastroenterol Hepatol. 2020;18:534–42.
2. Bray F, Laversanne M, Sung H, Ferlay J, Siegel RL. Global cancer statistics 2022: GLOBOCAN estimates of incidence and mortality worldwide for 36 cancers in 185 countries. CA Cancer J Clin. 2024;74:229–63.
3. Joshi SS, Badgwell BD. Current treatment and recent progress in gastric cancer. CA Cancer J Clin. 2021;71:264–79.
4. Seyfried TN, Huysentruyt LC. On the origin of cancer metastasis. Crit Rev Oncog. 2013;18:43–73.
5. Yamada D, Takao T, Nakamura M, Kitano T, Nakata E, Takarada T. Identification of surface antigens that define human pluripotent stem cell-derived PRRX1+limb-bud-like mesenchymal cells. Int J Mol Sci. 2022;23:2661.
6. Li A, Ma S, Smith SM, Lee MK, Fischer A, Borok Z, et al. Mesodermal ALK5 controls lung myofibroblast versus lipofibroblast cell fate. BMC Biol. 2016;14:19.
7. Takahashi Y, Sawada G, Kurashige J, Uchi R, Matsumura T, Ueo H, et al. Paired related homoeobox 1, a new EMT inducer, is involved in metastasis and poor prognosis in colorectal cancer. Br J Cancer. 2013;109:307–11.
8. Sun L, Han T, Zhang X, Liu X, Li P, Shao M, et al. PRRX1 isoform PRRX1A regulates the stemness phenotype and epithelial-mesenchymal transition (EMT) of cancer stem-like cells (CSCs) derived from non-small cell lung cancer (NSCLC). Transl Lung Cancer Res. 2020;9:731–44.
9. Chen Z, Chen Y, Li Y, Lian W, Zheng K, Zhang Y, et al. Prrx1 promotes stemness and angiogenesis via activating TGF-β/smad pathway and upregulating proangiogenic factors in glioma. Cell Death Dis. 2021;12:615.
10. Joko R, Yamada D, Nakamura M, Yoshida A, Takihira S, Takao T, et al. PRRX1 promotes malignant properties in human osteosarcoma. Transl Oncol. 2021;14:100960.
11. Li Y, Wang W, Wang F, Wu Q, Li W, Zhong X, et al. Paired related homeobox 1 transactivates dopamine D2 receptor to maintain propagation and tumorigenicity of glioma-initiating cells. J Mol Cell Biol. 2017;9:302–14.
12. Wang X, Yang R, Wang Q, Wang Y, Ci H, Wu S. Aberrant expression of vasculogenic mimicry, PRRX1, and CIP2A in clear cell renal cell carcinoma and its clinicopathological significance. Medicine (Baltimore). 2019;98:e17028.
13. Guo J, Fu Z, Wei J, Lu W, Feng J, Zhang S. PRRX1 promotes epithelial–mesenchymal transition through the Wnt/β-catenin pathway in gastric cancer. Med Oncol. 2015;32:393.
14. Yao J, Zhang Y, Xia Y, Zhu C, Wen X, Liu T, et al. PRRX1 promotes lymph node metastasis of gastric cancer by regulating epithelial-mesenchymal transition. Medicine (Baltimore). 2021;100:e24674.
15. Zhang Y, Yao J, Feng J, Wang S, Yang Z, Huang W, et al. Relationship between PRRX1, circulating tumor cells, and clinicopathological parameter in patients with gastric cancer. J BUON. 2020;25:1455–62.
16. You JS, Jones PA. Cancer genetics and epigenetics: two sides of the same coin?. Cancer Cell. 2012;22:9–20.
17. Baylin SB, Jones PA. A decade of exploring the cancer epigenome - biological and translational implications. Nat Rev Cancer. 2011;11:726–34.

18. Dawson MA, Kouzarides T. Cancer epigenetics: from mechanism to therapy. Cell. 2012;150:12–27.
19. Fang JY, Richardson BC. The MAPK signalling pathways and colorectal cancer. Lancet Oncol. 2005;6:322–7.
20. Lavoie H, Gagnon J, Therrien M. ERK signalling: a master regulator of cell behaviour, life and fate. Nat Rev Mol Cell Biol. 2020;21:607–32.
21. Marchand B, Pitarresi JR, Reichert M, Suzuki K, Laczkó D, Rustgi AK. PRRX1 isoforms cooperate with FOXM1 to regulate the DNA damage response in pancreatic cancer cells. Oncogene. 2019;38:4325–39.
22. Jiang J, Zheng M, Zhang M, Yang X, Li L, Wang S, et al. PRRX1 regulates cellular phenotype plasticity and dormancy of head and neck squamous cell carcinoma through miR-642b-3p. Neoplasia. 2019;21:216–29.
23. Feldmann K, Maurer C, Peschke K, Teller S, Schuck K, Steiger K, et al. Mesenchymal plasticity regulated by Prrx1 drives aggressive pancreatic cancer biology. Gastroenterology. 2021;160:346–361.e24.
24. Takano S, Reichert M, Bakir B, Das KK, Nishida T, Miyazaki M, et al. Prrx1 isoform switching regulates pancreatic cancer invasion and metastatic colonization. Genes Dev. 2016;30:233–47.
25. Takihira S, Yamada D, Osone T, Takao T, Sakaguchi M, Hakozaki M, et al. PRRX1-TOP2A interaction is a malignancy-promoting factor in human malignant peripheral nerve sheath tumours. Br J Cancer. 2024;130:1493–1504.
26. Huang X, Huang W, Wu K, Lin Q, Chen G. PRRX1/FOXM1 reduces gemcitabin-induced cytotoxicity by regulating autophagy in bladder cancer. Transl Androl Urol. 2022;11:1116–29.
27. Sun L, Liu L, Jiang J, Liu K, Zhu J, Wu L, et al. Transcription factor Twist1 drives fibroblast activation to promote kidney fibrosis via signaling proteins Prrx1/TNC. Kidney Int. 2024;106:840–55.
28. Johnston ALM, Lun X, Rahn JJ, Liacini A, Wang L, Hamilton MG, et al. The p75 neurotrophin receptor is a central regulator of glioma invasion. PLoS Biol. 2007;5:e212
29. Mochizuki M, Tamai K, Imai T, Sugawara S, Ogama N, Nakamura M, et al. CD271 regulates the proliferation and motility of hypopharyngeal cancer cells. Sci Rep. 2016;6:30707.
30. Chung MK, Jung YH, Lee JK, Cho SY, Murillo-Sauca O, Uppaluri R, et al. CD271 confers an invasive and metastatic phenotype of head and neck squamous cell carcinoma through the upregulation of Slug. Clin Cancer Res. 2018;24:674–83.
31. Wu R, Li K, Yuan M, Luo KQ. Nerve growth factor receptor increases the tumor growth and metastatic potential of triple-negative breast cancer cells. Oncogene. 2021;40:2165–81.
32. Zhang J, Ren Z, Zheng D, Song Z, Lin J, Luo Y, et al. AHSA1 promotes proliferation and EMT by regulating ERK/CALD1 axis in hepatocellular carcinoma. Cancers (Basel). 2022;14:4600.
33. Zhang G, Gao Z, Guo X, Ma R, Wang X, Zhou P, et al. CAP2 promotes gastric cancer metastasis by mediating the interaction between tumor cells and tumor-associated macrophages. J Clin Invest. 2023;133:e166224.
34. Du J, Lan T, Liao H, Feng X, Chen X, Liao W, et al. CircNFIB inhibits tumor growth and metastasis through suppressing MEK1/ERK signaling in intrahepatic cholangiocarcinoma. Mol Cancer. 2022;21:18.
35. Wang R, Huang W, Cai K, Xiao S, Zhang W, Hu X, et al. FLOT1 promotes gastric cancer progression and metastasis through BCAR1/ERK signaling. Int J Biol Sci. 2023;19:5104–19.
36. Li R, Han Z, Ma W, Zhang L, Zhang X, Jiang Y, et al. IMP4 silencing inhibits the malignancy of lung adenocarcinoma via ERK pathway. J Oncol. 2022;2022:8545441.
37. Liloglou T, Nikolaidis G. Quantitative methylation specific PCR (qMSP). Bio-protocol 3: e871. https://doi.org/10.21769/BioProtoc.871.
38. Li J, Ye D, Shen P, Liu X, Zhou P, Zhu G, et al. Mir-20a-5p induced WTX deficiency promotes gastric cancer progressions through regulating PI3K/AKT signaling pathway. J Exp Clin Cancer Res. 2020;39:212.